NEOPLASIA
www.neoplasia.com
Volume 22 Number xxx xxxx 2020 pp. 702–713

Original Research

The SRSF3-MBNL1-Acin1 circuit constitutes an emerging axis to lessen DNA fragmentation in colorectal cancer via an alternative splicing mechanism ☆

Yi-Su Chen [a,1]; Chao-Wei Liu [b,c,1]; Ying-Chin Lin [a,d]; Chia-Ying Tsai [e]; Ching-Hui Yang [e]; Jung-Chun Lin [b,e,f,*]

[a] Department of Family Medicine, Wan Fang Hospital, Taipei Medical University, Taipei, Taiwan
[b] Ph.D. Program in Medical Biotechnology, College of Medical Science and Technology, Taipei Medical University, Taipei, Taiwan
[c] Department of Laboratory Science, National Taiwan University Hospital, Taipei, Taiwan
[d] Department of Family Medicine, School of Medicine, College of Medicine, Taipei Medical University, Taipei, Taiwan
[e] School of Medical Laboratory Science and Biotechnology, College of Medical Science and Technology, Taipei Medical University, Taipei, Taiwan
[f] Pulmonary Research Center, Wan Fang Hospital, Taipei Medical University, Taipei, Taiwan

ABSTRACT

Altered alternative splicing (AS) events are considered pervasive causes that result in the development of carcinogenesis. Herein, we identified reprogrammed expression and splicing profiles of *Muscle blind-like protein 1* (*MBNL1*) transcripts in tumorous tissues compared to those of adjacent normal tissues dissected from individual colorectal cancer (CRC) patients using whole-transcriptome analyses. *MBNL1* transcript 8 (*MBNL1*$_8$) containing exons 5 and 7 was majorly generated by cancerous tissues and CRC-derived cell lines compared with those of the normal counterparts. Interplay between the exonic CA-rich element and upregulated SRSF3 facilitated the inclusion of *MBNL1* exons 5 and 7, which encode a bipartite nuclear localization signal (NLS) and conformational NLS. Moreover, abundant SRSF3 interfered with the autoregulatory mechanism involved in utilization of *MBNL1* exons 5 and 7, resulting in enrichment of the MBNL1$_8$ isoform in cultured CRC cell lines. Subsequently, an increase in the MBNL1$_8$ isoform drove a shift in the apoptotic chromatin condensation inducer in nucleus 1-S (Acin1-S) isoform to the Acin1-L isoform, leading to diminished DNA fragmentation in cultured CRC cells under oxidative stress. Taken together, SRSF3-MBNL1-Acin1 was demonstrated to constitute an emerging axis which is relevant to proapoptotic signatures and post-transcriptional events of CRC cells.

Neoplasia (2020) 22, 702–713

Keywords: Acin1, Alternative splicing, Colorectal cancer, MBNL, SRSF3

Introduction

Over 95% of human genes have been validated to transcribe more than one coding or noncoding transcript through alternative splicing (AS) mechanisms, which specify functions of human cells [1–3]. With the development of high-throughput sequencing approaches, a growing body of cancer genomics studies have revealed that aberrant AS is a pervasive phenomenon resulting in carcinogenic signatures, including immortalization and energy consumption [4,5]. In addition to a mutant *cis*-element which alters the strength of splicing sites, functional dysregulation or altered

* Corresponding author. School of Medical Laboratory Science and Biotechnology, College of Medical Science and Technology, Taipei Medical University, 250 Wu-Hsing Street, Taipei 11031.
E-mail address: lin2511@tmu.edu.tw (J.-C. Lin).
☆ Declaration of Competing Interest: All authors agree and declare that no conflict of interest exists.
[1] Yi-Su Chen and Chao-Wei Liu contributed equally to this work.
Received 17 August 2020; received in revised form 30 September 2020; accepted 4 October 2020

https://doi.org/10.1016/j.neo.2020.10.002

expression of splicing regulators frequently leads to cancer-associated AS events, which have been correlated with oncogenesis or loss-of-function in tumor suppression [6].

Colorectal cancer (CRC) is a frequently diagnosed malignancy and the third leading cause of cancer-mediated lethality worldwide [7]. Variations in genetic backgrounds were demonstrated to be related to the development and prognosis of CRC [8,9]. Correlations between altered AS events and progression of CRC have been widely documented in recent studies [10,11]. For instance, an increase in serine/arginine-rich splicing factor 3 (SRSF3) was recently demonstrated a potential oncogene toward development of CRC [12,13]. Further understanding of correlations between AS events involved in CRC development and their corresponding pathological signatures can be applied to develop predictive biomarkers or therapeutic targets in CRC patients.

Muscle blind-like 1 (MBNL1) is a well-characterized RNA-binding protein (RBP) that participates in regulating the development of multiple tissues [14–16]. MBNL1 was documented to regulate multiple post-transcriptional regulatory pathways, such as splicing, mRNA export, and mRNA degradation [17–19]. The functional specificity of MBNL1 was correlated with the conserved $CX_7CX_{4-6}CX_3H$ zinc finger which serves as RNA-binding domains (RBDs) and nuclear localization signals (NLSs) that determine its binding tendency and subcellular localization [19]. The interplay between RBDs within the MBNL1 protein and a corresponding RNA motif consisting of a GC dinucleotide flanked by pyrimidines (YGCY) was recently identified [20]. Result of a transcriptome-based analysis further indicated the necessity of single-stranded pyrimidines for MBNL binding [20]. AS exons 1, 5, and 7 within *MBNL1* transcripts constitute an autoregulatory mechanism for manipulating its expressions, splicing profiles, and biological functions [19–21]. In addition to the molecular mechanism involved in regulating MBNL1 and MBNL1-mediated impacts on tissue development, its influence on carcinogenesis was recently investigated. MBNL1 exerted potential effect on suppressing the progression of breast cancer and CRC possibly through AS regulation [22–24].

In the present study, discriminative expression and splicing profiles of *MBNL1* transcripts were identified in paired CRC cancerous/adjacent normal tissues using whole-transcriptome assays. In addition to reduced expressions of total MBNL1, the SRSF3-mediated increase in the $MBNL1_8$ isoform further reduced the suppressive effect of the MBNL1 protein on DNA fragmentation in CRC cells by programming relative levels of the apoptotic chromatin condensation inducer in the nucleus (Acin1)-L isoform.

Materials and methods

Ethics statement of patient samples and cell culture

This study was approved by the Joint Institutional Review Board of Taipei Medical University (TMU; approval no. 201,409,044). Human colorectal tumor samples ($n = 20$) were purchased as anonymous specimens from the TMU Joint Biobank with informed consent. Experiments with clinical specimens were conducted in accordance with relevant guidelines. HCT-8, Colo205, HCT-116, and Caco2 cells were cultured in RPMI-1640 medium supplemented with 10% fetal bovine serum (FBS), 600 mg/mL glutamine, 100 U/mL penicillin, and 100 mg/mL streptomycin (Invitrogen, Camarillo, CA, USA).

Total RNA extraction, RNA sequencing, and bioinformatics analysis

Total RNAs were extracted from clinical tissues using the PureLink RNA mini kit (Invitrogen) in accordance with the manufacturer's protocol. To minimize contamination by genomic DNA, extracted RNAs were treated with DNase I (Promega, Madison, WI, USA) prior to the following experiment. The integrity and quantity of RNAs for the whole-transcriptome assay were assessed using an Agilent 2100 Bioanalyzer (Agilent Technologies, Redwood, CA, USA) and Qubit 4 fluorometer (ThermoFisher Scientific, Carlsbad, CA, USA). Poly(A) mRNAs were enriched from 8 µg of total RNAs with a high integrity number (RIN of > 8.0) using oligo (dT)-based affinity matrices, followed by library construction using the NEB Next Ultra RNA Library Prep Kit from Illumina (NEB, Ipswich, MA, USA) according to the manufacturer's instructions. The prepared libraries were sequenced on an Illumina NextSeq 500 platform, and ~150-bp paired-end reads were generated. Preliminary reads were analyzed as reported in our previous study [25].The same batch of sequencing reads were reanalyzed using CLC genomics workbench (GWB) software (v.20.0.4; QIAGEN, Hilden, Germany) in this study. 50 × sequencing depth for human whole transcriptome analysis and the qualified Phred score (Q≧30) of mapped reads was subjected to analytic workflow.

Plasmid construction

The expression plasmid encoding the FLAG-tagged Acin1-L isoform (pCAGGS-Acin1-L) was a kind gift provided by Dr. Christian Schwerk (University of Mahhheim). The open reading frame (ORF) of the human Acin1-S isoform was amplified with a polymerase chain reaction (PCR) using a human fetal cDNA library as the template. The PCR product digested with *Hind* III/*BamH* I was inserted into the p3XFLAG-CMV14 vector (Sigma, St. Louis, MO, USA). ORFs of human MBNL1 isoforms 2 and 8 were amplified with a PCR using a human fetal cDNA library as the template. The PCR product digested with *Kpn* I/*BamH* I was inserted into the p3XFLAG-CMV14 vector (Sigma). The human genomic element containing the cassette exons of MBNL1 was PCR-amplified using human genomic DNA as the template. The PCR product was digested with *Kpn* I and *BamH* I restriction enzymes and inserted into pcDNA 3.1 vector (Invitrogen). Derived mutants of the splicing reporter or expressing vector containing the substituted nucleotide were constructed using the QuikChange site-directed mutagenesis system (Stratagene, Amsterdam, The Netherlands). Vector-based short hairpin (sh)RNAs targeting the human *MBNL1* or *Acin1* gene were purchased from the RNAi core facility at Academia Sinica (Taipei, Taiwan).

Transient transfection, reverse-transcription (RT)-PCR, and quantitative RT-(Q)PCR assays

CRC cell lines were grown to 60%~70% confluence, followed by plasmid transfection using Lipofectamine 3000 in accordance with the manufacturer's protocol (Invitrogen). Total RNAs were extracted using a PureLink RNA mini kit at 24 h post-transfection (Invitrogen). Total RNAs of 1 µg prepared from clinical tissues or cultured cells were reverse-transcribed using SuperScriptase III (Invitrogen) in a 10-µL reaction. To identify alternatively-spliced transcripts, the reverse-transcribed product was subjected PCR assay using primer as listed in Supplementary Table 3. An RT-qPCR was performed with SYBR green fluorescent dye and gene-specific primer sets (Supplementary Table 4) using an ABI One Step PCR machine (Applied Biosystems, Foster City, CA, USA). The relative mRNA level was quantitated by the ΔΔ-Ct method, and normalized with the level of *GAPDH* transcripts.

Immunoprecipitation coupled RT-PCR assay

The transiently transfected cells were disrupted in 1% Nonidet P-40-containing RIPA buffer (10 mM sodium phosphate, 150 mM NaCl, 2 mM EDTA, pH 7.2), followed by anti-FLAG immunoprecipitation. The RNAs associated with FLAG-tagged protein were extracted with phenol-chloroform and precipitated with ethanol. The recovered RNAs were subsequently analyzed by RT-PCR as previously described.

Subcellular fractionation and immunoblot assay

The expressing vector encoding the FLAG-tagged MBNL isoform was transfected into HCT-116 cells using Lipofectamine 3000 (Invitrogen). Transient-transfected cells were collected and resuspended in 500 µL of RSB-100 buffer containing 40 mg/mL digitonin (Calbiochem, San Diego, CA, USA). After incubation on ice for 5 min, cells were centrifuged at 2000 *g* for 8 min. The supernatant was collected as the cytosolic fraction, and the pellet was resuspended in 500 µL of RSB-100 containing 0.5% Triton X-100 and incubated on ice. After centrifugation, the supernatant was collected as the nuclear fraction. The immunoblot analysis was conducted using an enhanced chemiluminescence (ECL) system (Millipore, Billerica, MA, USA), and results were monitored using the LAS-4000 imaging system (Fujifilm, Tokyo, Japan). Primary antibodies used in this study included monoclonal anti-FLAG M2 (dilution 1:2000; Sigma-Aldrich, St. Louis, MO, USA), monoclonal antiactin (dilution 1:4000; Chemicon, Millipore), monoclonal anti-SRSF3 (dilution 1:2000; Abnova, Taipei, Taiwan), polyclonal anti-GAPDH (dilution 1:2000; MDBio, Taipei, Taiwan), polyclonal anti-α Tubulin (dilution 1:2000; Abcam, Cambridge, UK), polyclonal anti-Acin1 (dilution 1:1000; Cell Signaling Technology, MA, USA), polyclonal anti-MBNL1 (dilution 1:1000; Abcam, Cambridge, MA, USA; ab45899), and polyclonal antinucleolin (dilution 1:2000; Abcam, Cambridge, UK). Signal intensities were evaluated using TotalLab Quant Software.

In vitro *DNA fragmentation assay*

Transfected cells were grown in the presence of sodium arsenite in 6-cm dishes for 8 h. Cells were washed twice with phosphate-buffered saline (PBS) and lysed in 300 µL of lysis buffer (20 mM Tris-HCl at pH 7.4, 5 mM EDTA, 150 mM NaCl, and 0.5% Triton X100). After incubation on ice for 30 min, cells were centrifuged at 12,000 rpm for 15 min. RNaseA (200 µg/mL) was poured into the supernatant, and the mixture was incubated at 37 °C for 1 h. After the addition of proteinase K (200 µg/mL), the mixture was incubated at 37 °C for another 1 h. Fragmented DNA was extracted with phenol/chloroform/isoamyl alcohol (25:24:1 v/v/v) and precipitated with 95% ethanol. An equal amount of DNA was resolved in a 1% agarose gel and then stained with ethidium bromide (EtBr).

Cellular apoptosis assay

DeadEnd Fluorometric TUNEL system kit (Promega, Madison, WI, USA) was used to detect apoptotic cells. In brief, *in vitro* cultured cells were washed with cold PBSand then fixed with 4% paraformaldehyde for 30 min. Fixed cells were permeabilized by using 0.1% Triton X-100 and 0.1% Sodium citrate and next incubated with TUNEL assay mixture for 60 min. The TUNEL-stained cells were visualized using the Olympus IX81 microscope (Olympus, Tokyo, Japan).

Statistical analyses

Experimental results were analyzed using a one- or two-way analysis of variance (ANOVA) followed by Tukey's multiple-comparison post-hoc test. Analyzed results are expressed as the mean ± standard error of the mean (SEM) and considered significant at P values of <0.05 ($^{*}P < 0.05$; $^{**}P < 0.01$; $^{***}P < 0.005$).

Results

Genome-wide analyses identify reprogrammed expressions and splicing profiles of MBNL1 transcripts in CRC tissues

To identify the CRC-related AS profile, whole-transcriptome analyses were conducted with total RNA samples prepared from six pairs of cancerous and adjacent normal tissues which were dissected from independent CRC patients ($n = 6$) in our previous study [25]. As shown in Table 1A, a 2.8-fold decrease in total *MBNL1* transcripts was identified in cancerous tissues compared to adjacent normal tissues (Table 1A, multiple of change = 2.8144). In addition to expression levels, differential splicing profiles of *MBNL1* transcripts were characterized in independent paired tissues. Relatively low abundance of $MBNL1_2$ (Table 1B, NM_207,292; $\log_2$ multiple of change = −3.3683) with a concomitant increase in $MBNL1_8$ transcripts (Table 1B, NM_001314057; $\log_2$ multiple of change=3.2935) were identified in cancerous tissues compared to those of adjacent normal tissues. Nevertheless, expressions of $MBNL1_4$ transcripts (NM_207,294) and $MBNL1_6$ (NM_207,296) were not identified using a high-throughput sequencing approach.

As shown in Figure 1A, 9 AS transcripts transcribed from the human *MBNL1* gene were submitted to the National Center for Biotechnology Information (NCBI). To validate results of the whole-transcriptome assays, RT-PCR assays were subsequently conducted with total RNA samples prepared from paired cancerous and adjacent normal tissues dissected from independent CRC patients ($n = 11$). Exclusion of exon 5 or 7 was characterized in the majority of *MBNL1* transcripts ($MBNL1^{-ex\,5}$, $MBNL1^{+ex\,8}$, or $MBNL1^{-ex\,7/8}$) generated by normal colorectal tissues (Figure 1B, Normal; Clontech). Similar splicing profiles regarding the utilization of *MBNL1* exons 5 and 7 were identified in most adjacent normal tissues (Figure 1B, NT), whereas increases in the relative levels of $MBNL1^{+ex\,5}$ or $MBNL1^{+ex\,7/8}$ transcripts were observed in paired cancerous tissues (Figure 1B, T). In addition to clinical tissue samples, decreases in the relative levels of $MBNL1^{+ex\,5}$, $MBNL1^{+ex\,8}$, or $MBNL1^{+ex\,7/8}$ transcripts were observed in Caco2 cells (Figure 1C, lanes 1 and 4) derived from well-differentiated adenocarcinoma tissue [21]. In contrast, the majority of *MBNL1* transcripts generated by HCT-8 (Figure 1C, lanes 2 and 5) and HCT-116 (Figure 1C, lanes 3 and 6) CRC cancer cells were $MBNL1^{+ex\,5}$, $MBNL1^{+ex\,8}$, or $MBNL1^{+ex\,7/8}$. Moreover, relatively high levels of total *MBNL1* transcripts were noted in adjacent normal tissues (Figure 1D, NT) and Caco2 cells (Figure 1E, lane 1) compared to those of cancerous tissues (Figure 1D, T), HCT-8, or HCT-116 cells (Figure 1E, lanes 2 and 3). These results demonstrated the reprogrammed expressions or splicing profiles of *MBNL1* transcripts in CRC tissues or derived cell lines compared to those in adjacent normal tissue or well-differentiated cells.

Utilization of exons 5 and 7 is relevant to the biological properties of MBNL1 isoforms

The property of the respective MBNL1 isoforms in relation to splicing activity, such as subcellular localization, was first evaluated in this study. The nuclear index was applied to present subcellular localization of the FLAG-tagged MBNL1 isoform in transient transfectants. The majority of the overexpressing $MBNL1_8$ isoform containing the NLS encoded by exons 5 and 7 was identified in the nuclear fraction (Figure 2A, lane 1, nuclear index = 0.7827). In contrast, the absence of exon 5 or 7 may be relevant to a decrease in the nuclear deposition of FLAG-tagged $MBNL1_2$ (Figure 2A, lane 3, nuclear index = 0.4221) compared to that of the $MBNL1_8$ isoform. The potential impact of the MBNL1 isoform with discriminative subcellular localization on AS events was examined using an *in vitro* culture system. Using RT-PCR assays, the presence of overexpression of the $MBNL1_2$ isoform was shown to drive the splicing profiles of *insulin receptor* (*INSR*) and *fibroblast growth receptor 2* (FGFR2), genes to noncarcinogenic *INSR-B* and *FGFR2-IIIb* transcripts (Figure 2B, lane 3) compared to those of empty vector (EV)-transfected HCT-116 cells (Figure 2B, lane 1) [26,27]. In contrast, overexpression of $MBNL1_8$ resulted in further increases in relative levels of *INSR-A* and *FGFR2-IIIc* transcripts (Figure 2B, lane 2) as observed in the HCT-116 CRC cell line (Figure 2B, lane 1). Predominant expressions of *INSR-A* and *FGFR2-IIIc* transcripts were consistently evaluated using whole-transcriptome assays with total RNAs

Table 1

Genome-wide analyses reveal reprogrammed muscle blind-like protein 1 (*MBNL1*) transcript levels in colorectal cancer (CRC) tissues and adjacent normal tissues. Total RNAs prepared from six pairs of independent tissues ($n = 6$) were subjected to whole-transcriptome analyses, the sequencing results of which were analyzed using CLC genomics workbench (GWB) software (v.20.0.4). (a) Gene expressions and (b) transcript profiles of *MBNL1* were identified in cancerous (T) and paired normal (NT) tissues.

a

Gene	Locus	sample_1	sample_2	FPKM_1	FPKM_2	log2(T/NT)	*p*_value	*q*_value
MBNL1	chr3:152243828-152465780	CRC-NT	CRC-T	15.6726	9.45013	-1.492827	4.168E-05	0.015

b

Sample	Gene	Accesion No.	ENSEMBL	Isoform	FPKM	TPM	$\log_2$(T/NT)	*p*_value	FDR *p*_value
NT	MBNL1	NM_021038	ENST00000324210	$MBNL1_1$	0.2468	0.4154	-0.0292	0.8126	0.9998
	MBNL1	NM_207292	ENST00000355460	$MBNL1_2$	1.6138	2.91463	-3.3683	1.11E-5	3.3E-4
	MBNL1	NM_207293	ENST00000463374	$MBNL1_3$	0.756	1.8772	-0.8814	1.66E-3	2.78E-2
	MBNL1	NM_207295	ENST00000459747	$MBNL1_5$	0.1664	0.2801	-0.8487	0.0143	0.0464
	MBNL1	NM_207296	ENST00000324196	$MBNL1_6$	0	0	N/A	N/A	N/A
	MBNL1	NM_207297	ENST00000357472	$MBNL1_7$	1.1333	1.907	-0.6048	0.11	0.74
	MBNL1	NM_001314057	ENST00000493459	$MBNL1_8$	2.7436	4.7914	3.2925	1.18E-5	1.86E-2
	MBNL1	NM_001363870	ENST00000498502	$MBNL1_9$	0.6311	1.7446	0.8056	0.4401	0.8722
T	MBNL1	NM_021038	ENST00000324210	$MBNL1_1$	0.1997	0.4091			
	MBNL1	NM_207292	ENST00000355460	$MBNL1_2$	0.691	1.1628			
	MBNL1	NM_207293	ENST00000463374	$MBNL1_3$	0.628	1.7913			
	MBNL1	NM_207295	ENST00000459747	$MBNL1_5$	0.1438	0.1438			
	MBNL1	NM_207296	ENST00000324196	$MBNL1_6$	0	0			
	MBNL1	NM_207297	ENST00000357472	$MBNL1_7$	1.191	2.1506			
	MBNL1	NM_001314057	ENST00000493459	$MBNL1_8$	8.7436	15.7914			
	MBNL1	NM_001363870	ENST00000498502	$MBNL1_9$	0.884	2.2094			

prepared from cancerous tissue samples compared to those of adjacent normal tissues as shown in Supplementary Table 1 ($n = 6$). Taken together, the influence of the respective MBNL1 isoform on AS events was manipulated by utilizing *MBNL1* exons 5 and 7 which might be relevant to its subcellular localization.

Utilization of MBNL1 exons 5 and 7 is modulated through an autoregulatory mechanism

Autoregulated selection of *MBNL1* exon 1, 5, or 7 was previously uncovered in diverse circumstances [20,21,28]. Nevertheless, we wondered whether the AS MBNL1 isoform exhibited a discriminative influence on the selection of its own exons as occurs with programming of other CRC-related splicing events. Depletion of endogenous MBNL1 consistently resulted in further inclusion of *MBNL1* exon 5 (Figure 3A, lanes 3 and 4; upper) or *MBNL1* exon 7 (Figure 3A, lanes 3 and 4; lower) in CaCo2 or HCT-116 cells compared to those of empty vector (EV)-transfected cells (Figure 3A, lanes 1 and 2). Overexpression of FLAG-tagged $MBNL1_8$ exhibited a more-prominent effect (Figure 3B, lane 2) than did overexpression of the $MBNL1_2$ isoform (Figure 3B, lane 3) on enhancing generation of $MBNL1^{-ex5}$ (Figure 3B, upper) or $MBNL1^{-ex7}$ (Figure 3B, lower) compared to those of empty vector transfectants (Figure 3B, lane 1). Supplementation of FLAG-tagged $MBNL1_8$ isoform antagonized the impact of MBNL1 depletion on enhancing inclusion of *MBNL1* exon 7 (Figure 3B, lanes 5 and 6). Accordingly, more exon 5- or 7-skipped transcripts were generated by the respective *in vitro* splicing reporter with overexpression of the $MBNL1_8$ isoform (Figure 3C, lane 2) compared to those of EV transfectants (Figure 3C, lane 1). Splicing patterns of splicing minigenes consistently showed an insubstantial response to the presence of the $MBNL1_2$ isoform (Figure 3C, lane 3). These results demonstrated that MBNL1 isoforms constituted an autoregulatory mechanism toward utilization of its own exons 5 and 7 even in a carcinogenic environment.

An increase in SRSF3 antagonizes the autoregulatory effect of MBNL1 on its own splicing profiles

In addition to autoregulation, *MBNL1* splicing was reprogrammed with an increase in SRSF3 which functions as an oncogenic regulator in osteosarcoma cells [29]. Putative motifs of SRSF3, CA(G/C/A)CC(C/A) or CCAGC(G)C, were noted in*MBNL1* exons 5 and 7 as shown in Figure 4A [27]. A loss-of-function approach was first applied to evaluate the regulatory impact of SRSF3 on utilization of *MBNL1* exons 5 or 7. Introduction of respective targeting vectors led to depletion of the endogenous SRSF3 protein with a concomitant increase in relative levels of $MBNL1^{-ex5}$ (Figure 4B, upper, lanes 2 and 3) or $MBNL1^{-ex7/8}$ (Figure 4B, lower, lanes 2 and 3) compared to those of EV transfectants (Figure 4B, lane 1). In contrast, overexpression of FLAG-tagged SRSF3 drove a shift in the $MBNL1^{-ex5}$ or $MBNL1^{-ex7/8}$ transcripts to $MBNL1^{+ex5}$ or $MBNL1^{+ex7/8}$ transcripts (Figure 4C, lane 2), whereas splicing profiles of the endogenous *MBNL1* gene showed no response to the presence of the engineered SRSF3 mutant containing a serine–to-alanine (S30A) substitution (Figure 4C, lane 3) compared to that of EV-transfected cells (Figure 4C, lane 1). Since SRSF3 and the $MBNL1_8$ isoform exerted opposite influences on selection of *MBNL1* exons 5 and 7, we subsequently evaluated whether SRSF3 alleviated autoregulation of *MBNL1* splicing. As shown in Figure 4D, gradual increases in FLAG-tagged SRSF3 reversed MBNL1-induced skipping of *MBNL1* exon 5 or 7 in a dose-dependent manner (Figure 4D, lanes 3 to 5) compared to that of MBNL1-overexpressing cells (Figure 4D, lane 2). This result suggested direct inhibition of SRSF3 on autoregulation of *MBNL1* splicing.

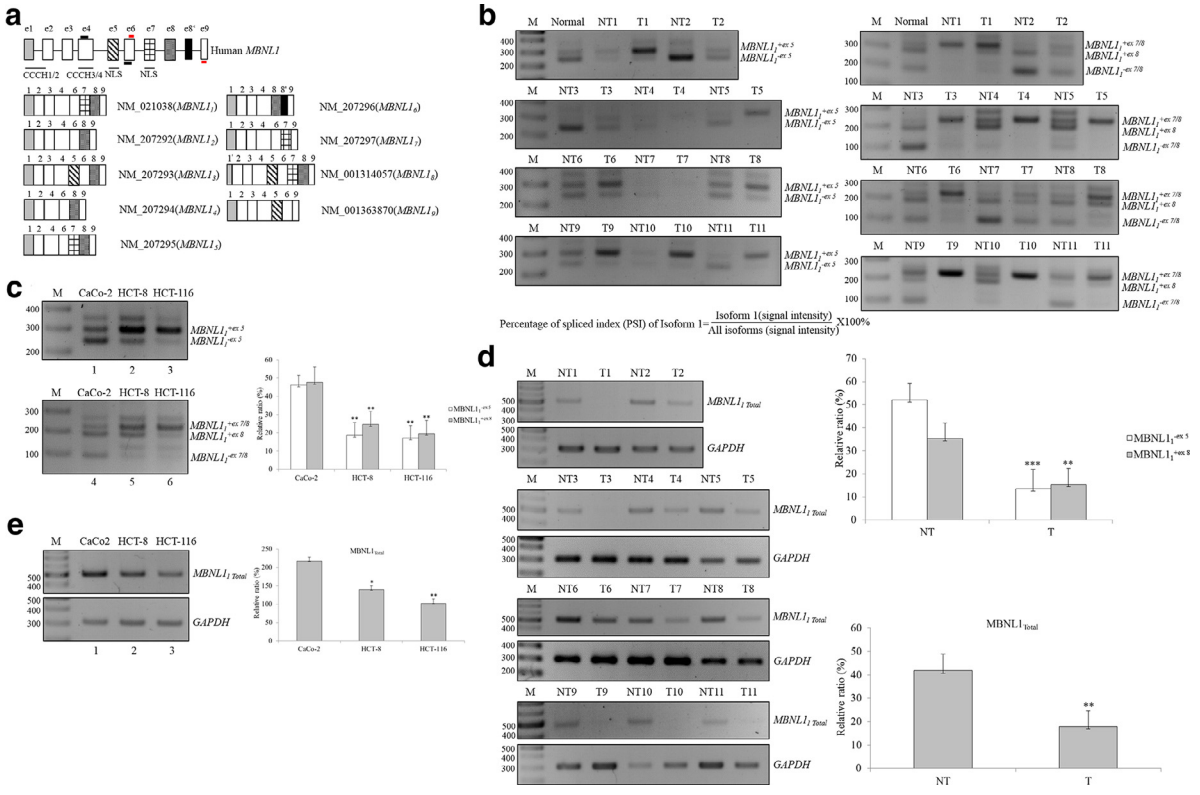

Figure 1. Reprogrammed expressions of total and alternatively-spliced muscle blind-like protein 1 (*MBNL1*) transcripts in colorectal cancer (CRC) tissues and cell lines. (a) The diagram presents the exonic compositions of *MBNL1* transcripts. (b) Total RNAs prepared from human colon tissue (Normal), or independent pairs of cancerous (T) and adjacent normal tissues (NT; $n = 11$) were subjected to RT-PCR assays using specific primers as labeled in Figure 1a (black and red lines) and listed in Supplementary Table 3. (c) Total RNAs isolated from CRC-derived cell lines were subjected to RT-PCR assays using specific primer sets as described in section (b). (D and E) Expressions of the total *MBNL1* transcripts in independent pairs of cancerous (T) and adjacent normal tissues (NT; $n = 11$), or CRC-derived cell lines were monitored using RT-PCR analyses with specific primers as listed in Supplementary Table 3. Signal densities of the RT-PCR results were quantified using TotalLab Quant Software. Quantitative results are shown as the mean ± SD. Statistical significance between independent samples was determined using a one-way ANOVA with Tukey's post-hoc analysis (*$P < 0.05$; **$P < 0.01$).

SRSF3 and MBNL1 antagonistically modulate the selection of MBNL1 exons in a sequence-dependent manner

The binding tendency of MBNL1 to responsive elements, including CHG (H corresponds to A, C, or U) or YGCY, was previously demonstrated using diverse approaches [30–33]. To pursue the detailed mechanism regarding SRSF3- and MBNL1-regulated utilization of *MBNL1* exons 5 and 7, a canonical splicing reporter containing cassette exons of *MBNL1* and derived mutants were constructed and applied in subsequent assays (Figure 5A). Disruption of the SRSF3-responsive motif (CAACC to CATCC) interfered with the production of $MBNL1^{+ex5}$ transcripts generated by the M1 reporter (Figure 5B, upper, lane 2), whereas more $MBNL1^{+ex5}$ transcripts were generated by the M2 reporter (Figure 5B, upper, lane 3) which contained the mutant MBNL1 responsive motif (CCTG to CCAG) compared to that of the wild-type (WT) MBNL1 ex5 reporter (Figure 5B, upper, lane 1). An adenosine-to-thymine substitution within the CACCC motif led to a decrease in relative levels of $MBNL1^{+ex7}$ transcripts generated by the M3 mutant reporter (Figure 5B, lower, lane 2), whereas a cytosine-to-guanine substitution within the CGCT motif further strengthened the production of $MBNL1^{+ex7}$ transcripts transcribed by the M4 mutant reporter (Figure 5B, lower, lane 3) compared to that of the WT MBNL1 ex7 reporter (Figure 5B, lower, lane 1).

As shown in Figure 5C, results of the *in vitro* splicing assay showed that overexpression of the FLAG-tagged SRSF3 and $MBNL1_8$ protein exhibited opposite influence on inclusion of *MBNL1* exon 5 (Figure 5C, upper lanes 2 and 3) or exon 7 (Figure 5C, lower, lanes 2 and 3) compared to those of empty vector-transfected cells (Figure 5C, lane 1). Disruption of the *SRSF3*-responsive element within *MBNL1* exon 5 or exon 7 interfered with the impact of overexpressing SRSF3 on enhancing inclusion of *MBNL1* exon 5 or exon 7 (Figure 5C, lane 5) compared to those of EV-cotransfected cells (Figure 5C, lane 4). In contrast, splicing profiles of the M2 or M4 reporter containing the interrupted MBNL1 motif exhibited a minor response to the presence of overexpression of the $MBNL1_8$ isoform (Figure 5C, lane 9). The results of immunoprecipitation-coupled RT-PCR indicated the respective association of FLAG-tagged $MBNL1_8$ with *MBNL1* exon 5-skipped transcripts (Figure 5D, lane 2) or FLAG-tagged SRSF3 with *MBNL1* exon 5-included transcripts (Figure 5D, lane 3). Disruption of SRSF3 or $MBNL1_8$ binding motif interfered with the association of SRSF3 or $MBNL1_8$ with spliced transcripts generated from the M1 (Figure 5D, lane 6) or M2 reporter (Figure 5D, lane 9) as compared to those of WT reporter (Figure 5D, lanes 2 and 3). Taken together, the interplay among SRSF3, MBNL1, and the corresponding motif constituted an antagonistic mechanism toward the utilization of *MBNL1* exon 5 and exon 7.

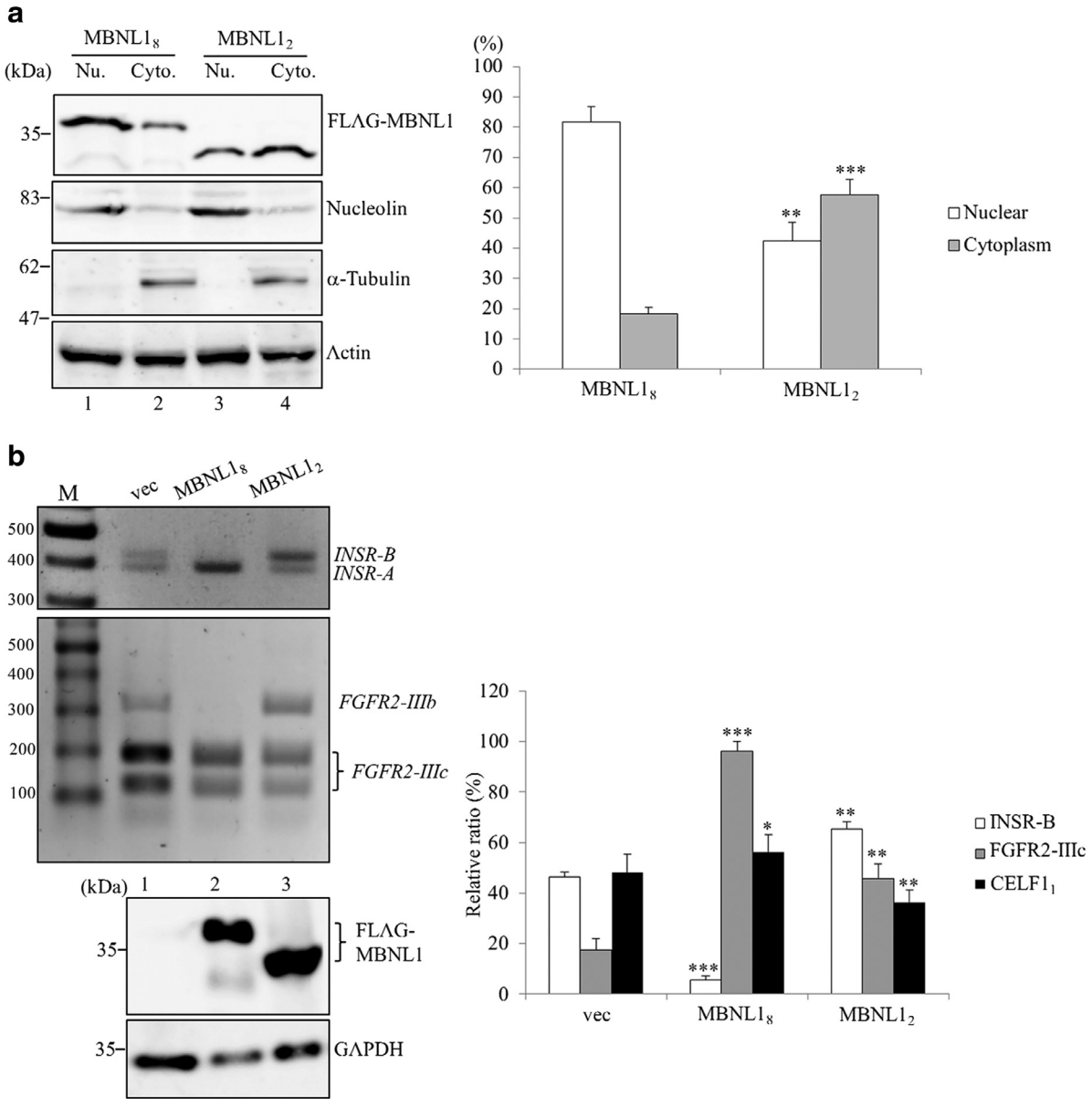

Figure 2. Subcellular localization of the muscle blind-like protein 1 (MBNL1) isoform is relevant to its influence on regulation of alternative splicing (AS) events. (a) HCT-116 cells were transfected with a vector expressing the MBNL1 isoform. Subcellular fractions were prepared from transfected cells, and analyzed with an immunoblot assay using primary antibodies against FLAG tag, nucleolin, α-Tubulin, and actin ($n = 4$). (b) A vector expressing the MBNL1 isoform was transfected into HCT-116 cells. After 24 h, total RNAs were extracted from transient transfectants and subjected to RT-PCR assays using specific primer sets as listed in Supplementary Table 3 ($n = 4$). Quantitative results of alternatively-spliced transcripts are shown as the mean ± SD. Statistical significance between independent samples was determined using a one-way ANOVA with Tukey's post-hoc analysis. ($^*P < 0.05$; $^{**}P < 0.01$; $^{***}P < 0.005$).

Abundance of the Acin1 isoform is relevant to expressions of SRSF3 and MBNL1 isoforms

The MBNL1 Δex7 isoform was reported to cause DNA damage, which diminished carcinogenic signatures, including cell viability [24]. Among apoptosis-related factors, apoptotic chromatin condensation inducer 1 (also referred as Acin1; NC_000014) was multifunctionally involved in caspase-3-induced chromatin condensation and splicing regulation with SAP18 and RNPS1, which was termed the apoptosis and splicing-associated protein (ASAP) [34,35]. Sustained expressions of total *Acin1* transcripts in tumorous and adjacent normal colonic tissues were noted from results of RNA sequencing (Supplementary Table 2A; $n = 6$). Nevertheless, a decrease in *Acin1-L* transcripts with a concomitant increase in *Acin1-S* transcripts was identified in adjacent normal tissues (Supplementary Table 2B) compared to those of CRC tissues. Upregulated levels of *Acin1-L* transcripts were further validated in CRC tissues (Figure 6A, white bar; $n = 11$), whereas relatively abundant expressions of *Acin1-S* transcripts were identified in adjacent normal tissues (Figure 6A, black bar) using quantitative (q)RT-PCR assays. Relatively high levels of *Acin1-S* transcripts with concomitant low expressions of *Acin1-L* transcripts were identified in Caco2 cells (Figure 6B,

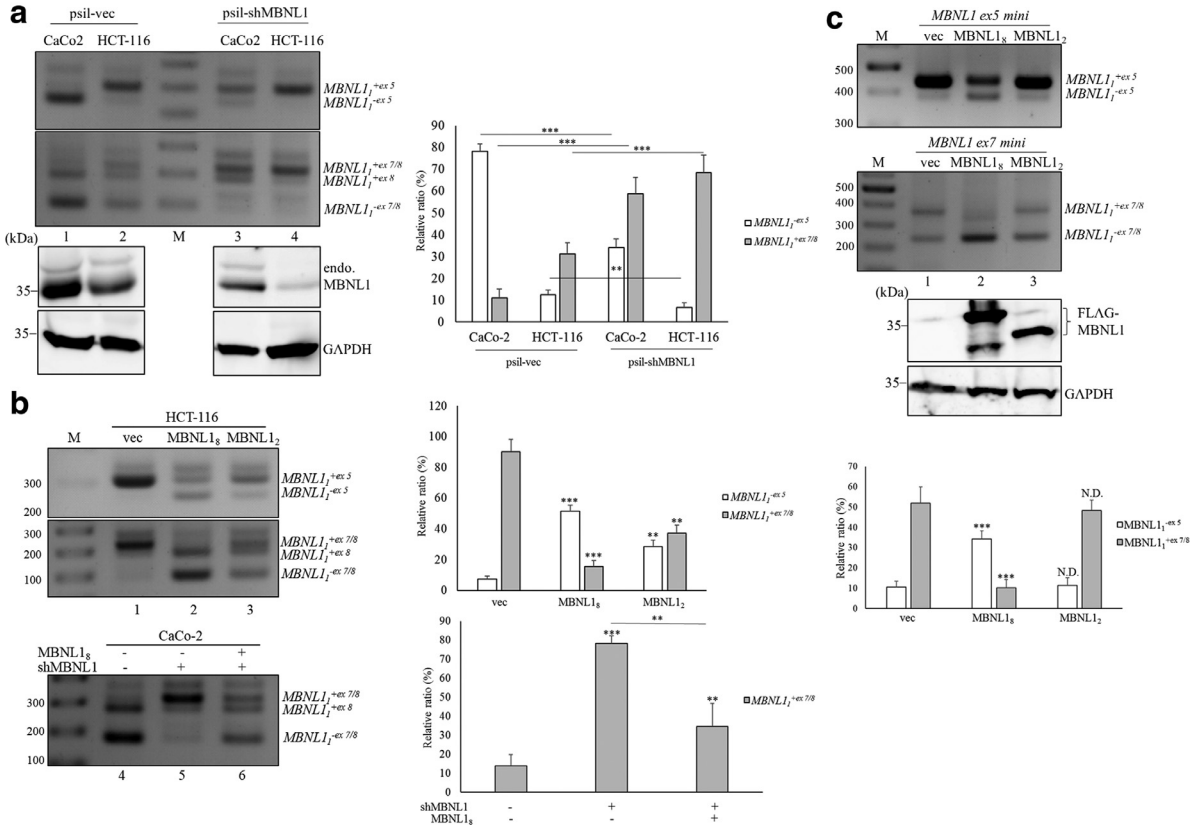

Figure 3. Overexpression of the muscle blind-like protein 1 (MBNL1) isoform differentially lessens exclusion of alternatively spliced MBNL1 exons. (A) Caco2 and HCT-116 cells were transfected with a targeting vector against total MBNL1. After 24 h, total RNAs and cell lysates were extracted and subjected to RT-PCR and immunoblot assays using specific primer sets and indicated antibodies. (b) An empty vector, overexpressing vectors of $MBNL1_8$ or $MBNL1_2$, or targeting vector of MBNL1 were sole- or cotransfected into HCT-116 cells. After 24 h, total RNAs and cell lysates were extracted and subjected to RT-PCR assays as previously described. (c) The *in vitro MBNL1* splicing reporter was cotransfected with expression vectors encoding $MBNL1_8$ or $MBNL1_2$ in HCT-116 cells. Total RNA and cell lysates were prepared at 24 h post-transfection and subjected to parallel RT-PCR and immunoblot assays as previously described. Quantitative results are shown as the mean ± SD ($n = 4$). Statistical significance between independent samples was determined using a one-way ANOVA with Tukey's post-hoc analysis ($^*P < 0.05$; $^{**}P < 0.01$; $^{***}P < 0.005$).

lane 1) compared to HCT-8 and HCT-116 cells (Figure 6B, lanes 2 and 3). Targeting of endogenous SRSF3 mediated a shift in the *Acin1-L* to *Acin1-S* transcripts (Figure 6C, lane 2), whereas depletion of total MBNL1 proteins resulted in upregulation of *Acin1-L* transcripts (Figure 6C, lane 3) compared to EV-transfectants (Figure 6C, lane 1). Conversely, the presence of FLAG-tagged SRSF3 drove an increase in relative levels of *Acin1-L* transcripts with a concomitant decrease in expressions of *Acin1-S* transcripts (Figure 6D, lane 2) compared to that of EV-transfectants (Figure 6D, lane 1). Overexpression of the exogenous $MBNL1_2$, but not the $MBNL1_8$, isoform exhibited opposite impacts as SRSF3 did on enhancing levels of *Acin1-S* transcripts (Figure 6D, lanes 3 and 4). The presence of FLAG-tagged $MBNL1_2$ consistently restored the relative abundance of $Acin1_S$ transcripts in MBNL1idepleted Caco-2 cells (Figure 6D, lanes 6 and 7), which further illustrated the influence of $MBNL1_2$ on the expression profile of *Acin1* gene. These results suggested that SRSF3 or MBNL1 exerted distinct influences on expressions of respective *Acin1* transcripts.

SRSF3-MBNL1-Acin1 constitutes a regulatory circuit involved in DNA fragmentation

Acin1 was demonstrated to be cleaved by caspase-3 throughout an apoptotic process, releasing p17 fragments to mediate chromatin condensation and oligonucleosomal DNA fragmentation [34]. Nevertheless, the impacts of distinct Acin1 isoforms on the apoptosis-related process are as yet uncharacterized. With exposure to sodium arsenite, more oxidative stress-mediated DNA fragmentation was only identified in HCT-116 cells that were transfected with the expression plasmid of FLAG-tagged Acin1-S (Figure 7A, lane 3) compared to that of Acin1-L overexpressing HCT-116 cells (Figure 7A, lane 2) or empty vector-transfected cells (Figure 7A, lane 1). DNA fragmentation was absent as well in Acin1-targeting cells with the treatment of arsenite (Figure 7A, lane 4). Consistently, more apoptotic cells were noted with the presence of FLAG-tagged $Acin1_S$ (Fig 7A, bar chart, $Acin1_S$). Targeting of oncogenic SRSF3 further strengthened the influence of arsenite treatment on inducing DNA fragmentation (Figure 7B, lane 2), whereas depletion of tumor-suppressive MBNL1 diminished levels of fragmented DNA under oxidative stress (Figure 7B, lane 3) compared to that of EV-transfectants (Figure 7B, lane 1). Depletion of SRSF3, but not MBNL1, led to an increase in the number of apoptotic cells (Fig 7B, bar chart, shSRSF3). As expected, overexpression of FLAG-tagged SRSF3 conversely interfered with the effect of arsenite on inducing DNA fragmentation (Figure 7C, lane 2) or apoptosis (Figure 7C, bar chart, SRSF3) in HCT-116 cells. The presence of overexpression of the $MBNL1_2$, but not the $MBNL1_8$, isoform, exerted an additive effect with arsenite treatment on mediating DNA fragmentation (Figure 7C, lanes 3 and 4) and apoptosis (Figure 7C, bar chart,

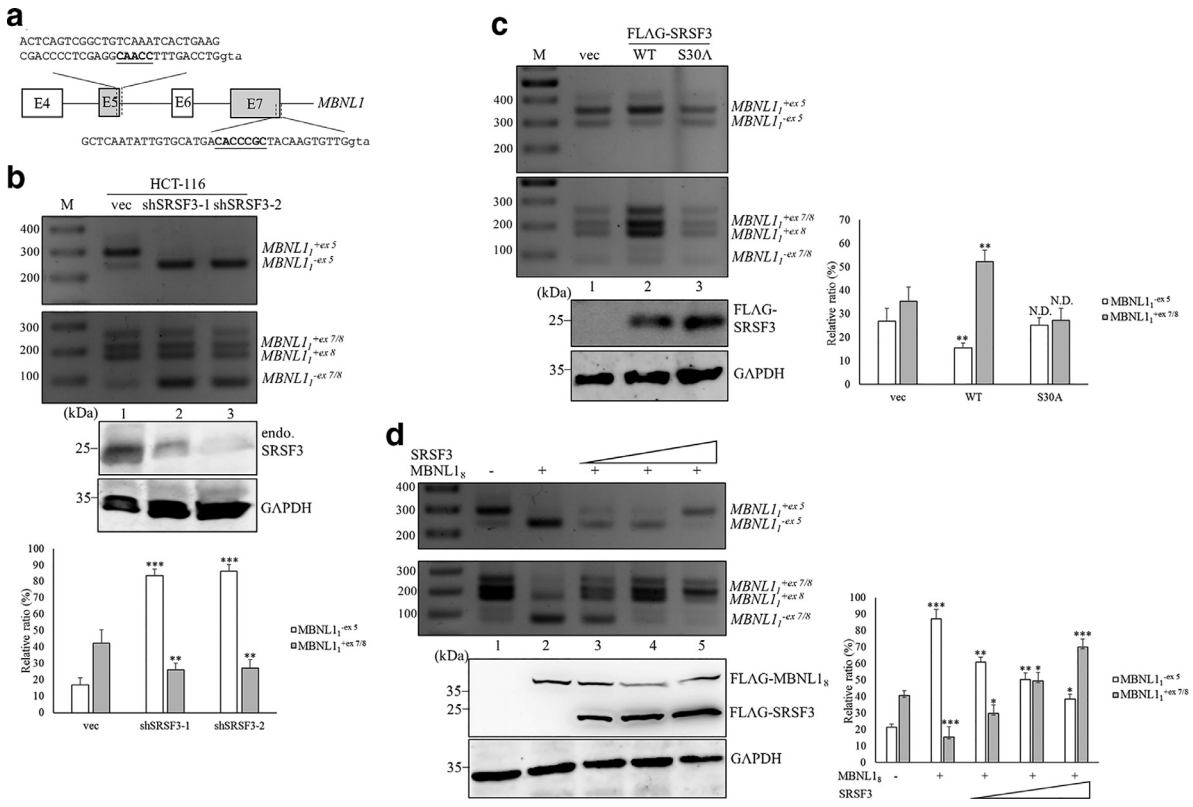

Figure 4. Upregulation of serine/arginine-rich splicing factor 3 (SRSF3) antagonizes the repressive influence of muscle blind-like protein 1 (MBNL1) on its own exons 5 and exon 7 in CRC cell lines. (a) The scheme presents the putative corresponding site of SRSF3 (underlined) within *MBNL1* exons 5 and 7. (b) A empty vector and a vector targeting endogenous *SRSF3* were transfected into HCT-116 cells, followed by incubation with growth medium for 24 h. Splicing profiles of *MBNL1* transcripts were analyzed using an RT-PCR approach ($n = 4$) with specific primer sets as listed in Supplementary Table 3. (c) An empty vector and a vector encoding the wild-type SRSF3 or an engineered mutant were transfected into HCT-116 cells, followed by incubation with growth medium for 24 h. Alternative splicing (AS) profiles of *MBNL1* transcripts were analyzed using an RT-PCR approach ($n = 4$) as described in the previous section. (d) An empty vector and a vector encoding the exogenous $MBNL1_8$ isoform were cotransfected with a gradually increasing amount of a vector encoding FLAG-tagged SRSF3. After 24 h, parallel RT-PCR analyses were performed to validate splicing profiles of *MBNL1* transcripts. Signal densities of the RT-PCR results were quantified using TotalLab Quant Software ($n = 4$). The bar graph presents relative levels of *MBNL1* transcripts. Quantitative results are shown as the mean ± SD. Statistical significance between independent samples was determined using a one-way (b) or two-way ANOVA (c and d) with Tukey's post-hoc analysis ($^*P < 0.05$; $^{**}P < 0.01$; $^{***}P < 0.005$).

$MBNL1_2$) compared to that of EV-transfected cells (Figure 7C, lane 1). As shown in Figure 7D, the results of TUNEL assay further demonstrated that overexpressing $MBNL1_2$ isoform respectively restored the apoptotic phenomenon in MBNL1-depleted cells (Figure 7D, left, $MBNL1_2$). Altered expression of SRSF3 and $MBNL1_2$ isoform exerted opposite influence on apoptosis of CRC cell with arsenite treatment (Figure 7D, middle). Moreover, an increase in $Acin1_L$ isoform lessened the cellular apoptosis in SRSF3-depleted or $MBNL1_2$-overexpressing cells (Figure 7D, right). These results suggested the influence of an emerging axis on manipulating the apoptotic activity of CRC cells.

Discussion

In mammalian cells, precise synergism of the spliceosome, transregulators, and corresponding *cis*-elements specifies spatiotemporal AS events which determine cellular functions [36]. Altered AS events are therefore considered a hallmark of carcinogenesis and are relevant to carcinogenic signatures [37]. In this study, distinct expressions or splicing profiles of *MBNL1* and *Acin1* transcripts were disclosed using whole-transcriptome analyses, which comprised a CRC-associated circuit involved in DNA fragmentation. The molecular mechanism involved in splicing regulation of MBNL1 was further pursued. The physiological relevance of the SRSF3-MBNL1-Acin1 cascade to apoptotic signatures, such as DNA fragmentation, of CRC-derived cells was subsequently demonstrated.

SRSFs constitute a well-characterized group which orchestrate diverse AS events and consequently coordinate gene expressions involved in various cellular processes [38]. In distinct malignancies, upregulated SRSF3 was identified as an oncogenic factor involved in active proliferation, transformation, and immortality by modulating AS profiles [39]. Depletion of endogenous SRSF3 was shown to facilitate the sensitivity of diverse cancer cells to apoptotic stress [40]. Altered level of SRSF3 in cancerous tissues or derived cells was predominantly related to an AS-coupled nonsense-mediated decay (NMD) pathway, which was demonstrated in numerous studies [41]. The interplay between SRSF3 and the corresponding exonic motif was previously demonstrated to enhance the yield of exon 16-included *mitogen-activated protein 4 kinase 4* (*MAP4K4*) transcripts, activating carcinogenesis-related signaling pathway [41]. In this study, the interplay between SRSF3 and the exonic CA motif functioned as a splicing enhancer toward the inclusion of *MBNL1* exon 5 or 7, which further demonstrated the impact of SRSF3-regulated mechanism involved in AS control.

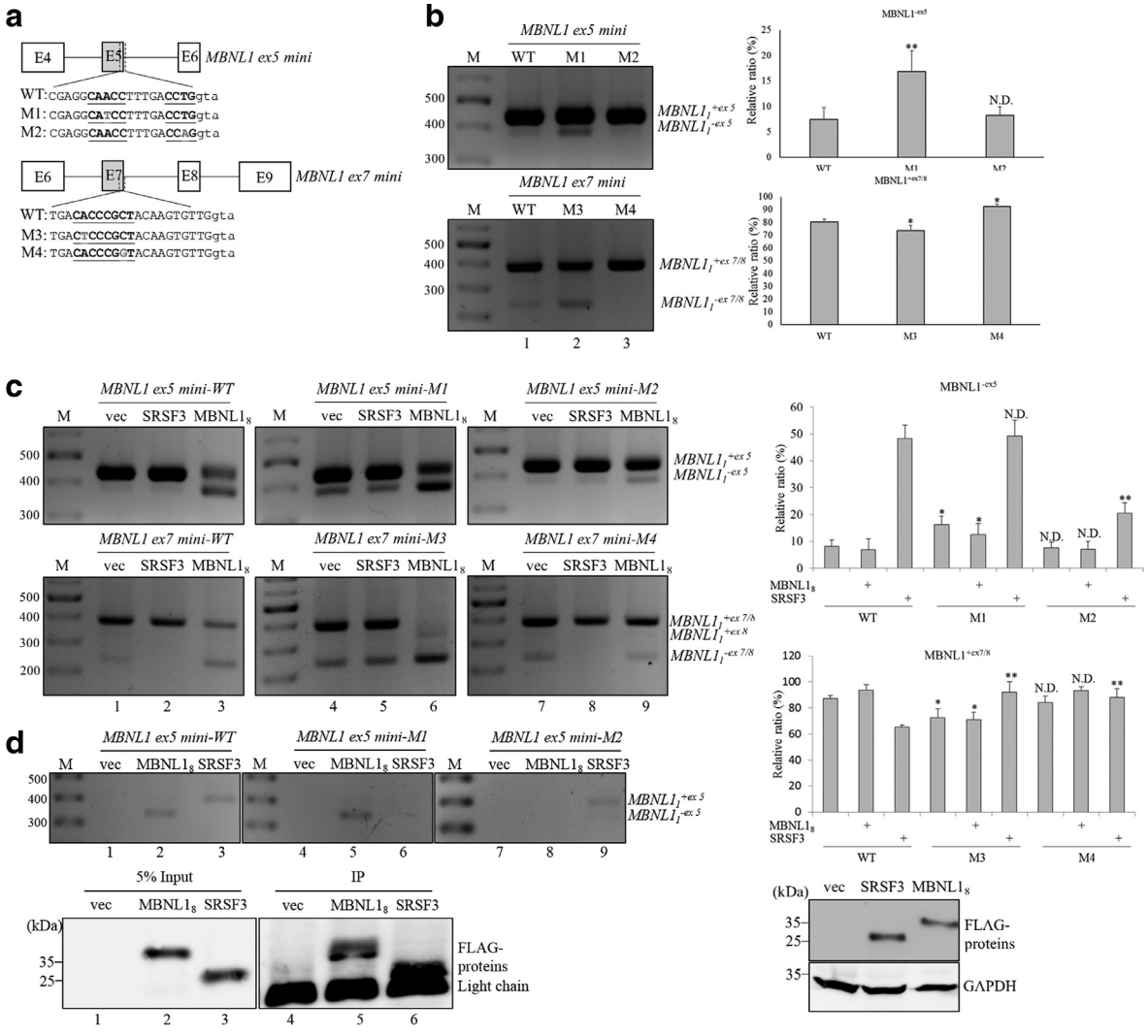

Figure 5. Serine/arginine-rich splicing factor 3 (SRSF3) and muscle blind-like protein 1 (MBNL1) orchestrate an antagonistic mechanism for selecting *MBNL1* exons 5 and 7 in a sequence-dependent manner. (a) The diagram presents the corresponding motif of *SRSF3* and *MBNL1* within the *MBNL1* splicing reporter and derived mutants. (b) The wild-type (WT) *MBNL1* splicing reporter or derived mutant was respectively transfected into HCT-116 cells. After 24 h, the splicing profile of the reporter was validated using RT-PCR assays ($n = 4$) with specific primer sets as listed in Supplementary Table 3. (c) The WT *MBNL1* splicing reporter or engineered mutants (M1 to M4) was cotransfected with the vector encoding SRSF3 or $MBNL1_8$ into HCT-116 cells. The splicing profile of the WT or mutant reporter was validated using RT-PCR assays ($n = 4$) as previously described. (d) The WT MBNL1 exon5 splicing reporter or engineered mutants was co-transfected with the vector encoding SRSF3 or MBNL18 into HCT-116 cells. The immunoprecipitated RNAs and proteins or extracted and subjected to RT-PCR or immunoblotting assays as previously described. Signal densities of the RT-PCR results were quantified using TotalLab Quant Software. Quantitative results are shown as the mean ± SD, and statistical significance between independent samples was determined using a one-way (b) or two-way (c) ANOVA with Tukey's post-hoc analysis (*$P < 0.05$; **$P < 0.01$; ***$P < 0.005$).

MBNL1 was demonstrated to be a master splicing regulator for shaping transcriptomic profiles throughout the development of striated muscle and blood lineages [42,43]. Even though the tumor-suppressive influence of MBNL1 toward cancer cells via AS regulation was recently revealed [23], the MBNL1 isoform was reported to exert an opposite effect on carcinogenic signatures [24]. The presence of the MBNL1 isoform lacking exon 7 was shown to cause DNA damage, which in turn interfered with cell viability and migration [24]. In this study, relatively high levels of exon 5- and exon 7-included $MBNL1_8$ transcripts were identified in cancerous tissues and derived cells using different approaches. Utilization of MBNL1 exons 7 and 8 participates in the coding of the bipartite NLS, whereas inclusion of MBNL1 exon 5 encoded a conformational NLS within the MBNL1 protein [21]. Interplay between MBNL1 and the intronic YGCY motif or exonic CCTG element exerted a coordinative impact on the skipping of *MBNL1* exon 5 [44,45]. In this study, MBNL1 acted as an exonic splicing silencer toward its own exon 7 in a YGCY motif-dependent manner. Accordingly, the autoregulatory mechanism for selection of MBNL1 exons 5 and 7 constitute a feedback loop to fine-tune the homeostasis of MBNL1 abundance and biological activities in nuclei. In CRC cell lines, abundant SRSF3 disturbed the autoregulation of *MBNL1* AS by interacting with the CA motif within *MBNL1* exon 5 or 7, consequently leading to continuous increases in $MBNL1_8$ transcripts. The potential impact of the SRSF3-MBNL1 axis on CRC-related AS events is worthy of further investigation.

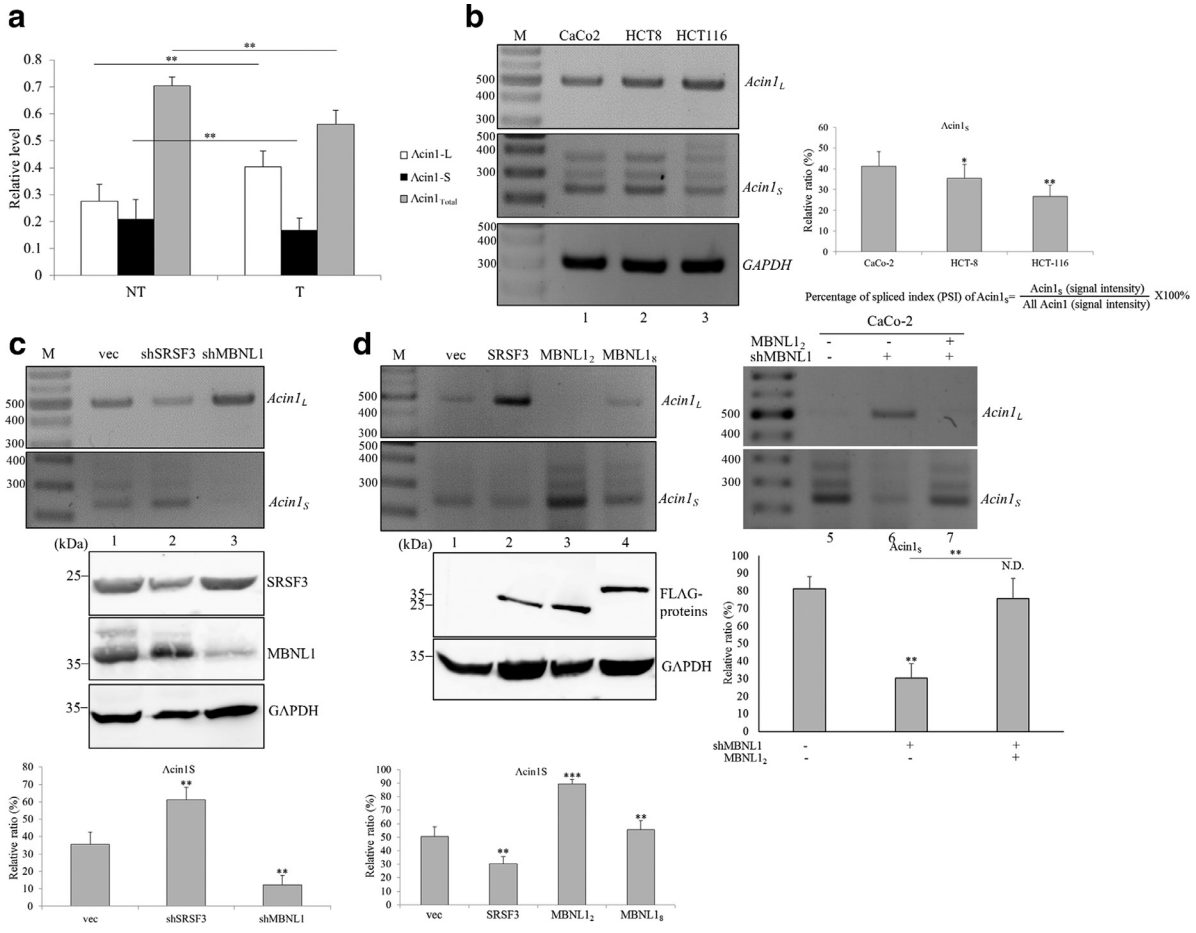

Figure 6. Expression profiles of apoptotic chromatin condensation inducer in the nucleus (Acin1) isoforms are differentially relevant to altered levels of serine/arginine-rich splicing factor 3 (SRSF3) and muscle blind-like protein 1 (MBNL1) isoforms in CRC cells. Total RNAs were extracted from (a) paired colonic tissues ($n = 11$) or (b) CRC-derived cell lines. Expression profiles of endogenous *Acin1* transcripts were analyzed using (a) qRT-PCR or (b) RT-PCR assays with specific primer sets listed in Supplementary Tables 3 and 4. (c) An empty vector and a vector targeting the endogenous *SRSF3* or *MBNL1* gene were transfected into HCT-116 cells, followed by incubation in growth medium for 24 h. Splicing profiles of *Acin1* transcripts were analyzed with RT-PCR assays ($n = 4$) as described in the last section. (d) An empty vector, overexpressing vectors of SRSF3, $MBNL1_8$, $MBNL1_2$, or targeting vector of MBNL1 were sole- or cotransfected into HCT-116 cells, followed by incubation in growth medium for 24 h. Parallel RT-PCR assays as previously described were performed to monitor splicing profiles of *Acin1* transcripts. Signal densities of the RT-PCR results were quantified using TotalLab Quant Software. Quantitative results are shown as the mean ± SD. Statistical significance between independent samples was determined using a one-way ANOVA with Tukey's post-hoc analysis ($^*P < 0.05$; $^{**}P < 0.01$; $^{***}P < 0.005$).

Acin1-L, Acin1-S, and *Acin1-S'* transcripts are transcribed from the *Acin1* gene through alternative promoter usage or an AS mechanism [46]. All Acin1 isoforms share an RNA recognition motif, RSB domain, and RS-rich region within its C-terminus, whereas the N-terminal SAP motif within Acin1-L mediates its interaction with AT-rich DNA regions [47,48]. Proteomic assays indicated the nuclear distribution of the Acin1-S and Acin1-S' isoforms, whereas the nuclear-cytoplasmic localization of the Acin1-L isoform was relevant to its SAP motif [47]. Even though Acin1 was first characterized as an RNA-binding protein involved in apoptosis, the influences of respective Acin1 isoforms on apoptotic signatures are uncharacterized [33]. Depletion of the endogenous Acin1 protein was reported to strengthen the sensitivity of cancerous cells toward apoptotic treatment [49]. Akt-mediated phosphorylation of Acin1-S was highly relevant to the generation of active p17 fragments involved in chromatin condensation, which is triggered by caspase 3-induced cleavage [34]. Overexpression of the Acin1-S isoform was first shown in this study to exhibit more-prominent efficiency than that of FLAG-tagged Acin1-L of inducing DNA fragmentation, which might be related to the distinct subcellular localization of the Acin1 isoform. In summary, upregulated SRSF3 disturbed autoregulation of MBNL1 splicing, leading to a continuous increase in $MBNL1_8$ transcripts. Increases in SRSF3 and $MBNL1_8$ shared a coordinated influence on enhancing relative levels of Acin1-L which exerted a less-efficient impact then did the Acin1-S isoform on DNA fragmentation and cellular apoptosis.

CRediT authorship contribution statement

Yi-Su Chen: Validation, Writing - original draft. **Chao-Wei Liu:** Validation, Writing - original draft. **Ying-Chin Lin:** Validation, Writing - original draft. **Chia-Ying Tsai:** Validation. **Ching-Hui Yang:** Validation. **Jung-Chun Lin:** Conceptualization, Methodology, Formal analysis, Resources, Writing - original draft, Supervision, Project administration, Funding acquisition.

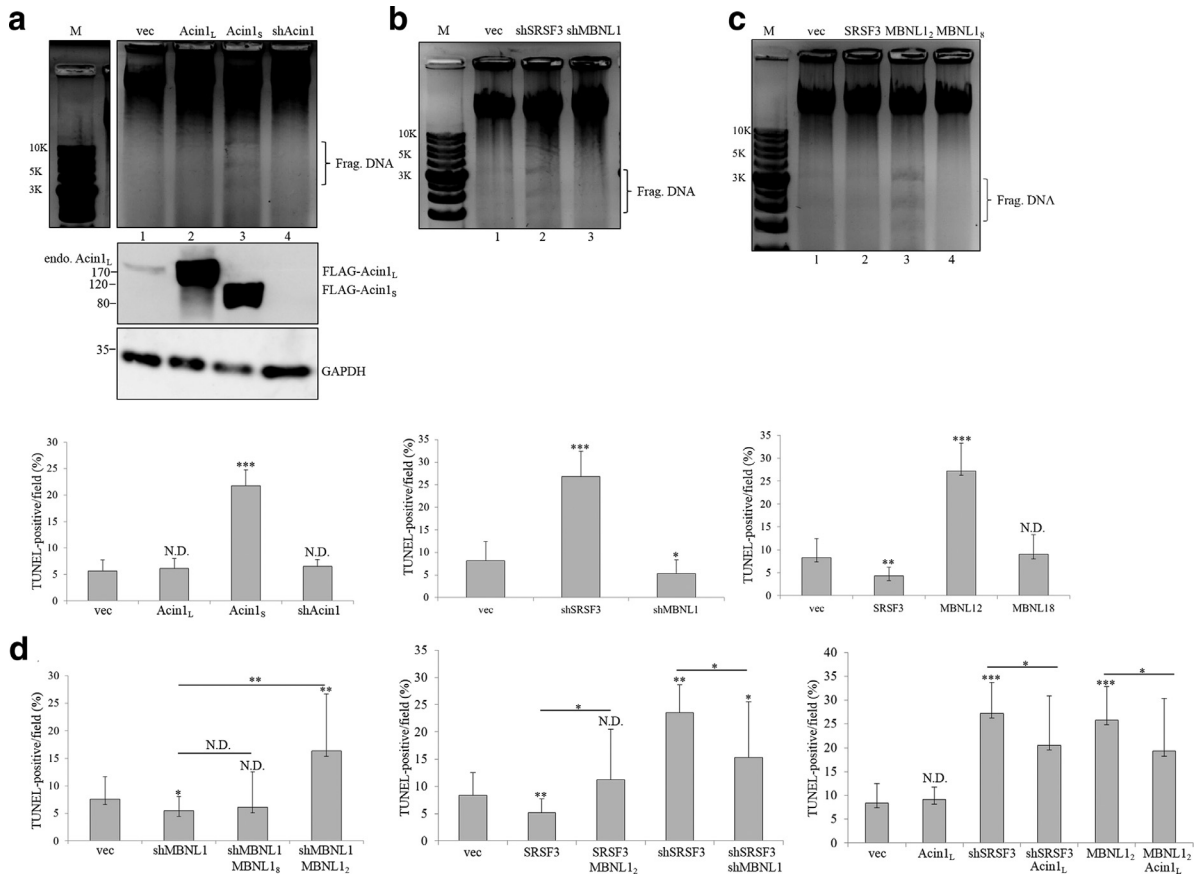

Figure 7. Apoptotic chromatin condensation inducer in the nucleus (Acin1) isoform exhibits differential impacts on apoptotic signature in CRC cells. (a) An empty vector, vector encoding the Acin1-L or Acin1-S isoform, or targeting vector of Acin1 were transfected into HCT-116 cells, followed by incubation in growth medium supplemented with sodium arsenite (25 μM) for 24 h. Extracted genomic DNA was subsequently digested with an RNase cocktail and proteinase K, followed by agarose gel electrophoresis. Parallel transfectants were synchronously subjected to TUNEL analyses. HCT-116 cells were transfected with an empty vector and a vector targeting SRSF3 or muscle blind-like protein 1 (MBNL1) (b) or a vector encoding SRSF3 or MBNL1 isoforms (c), followed by incubation in growth medium supplemented with sodium arsenite (25 μM) for 24 h. Parallel DNA fragmentation assays and TUNEL analysis were conducted as previously described. (d) An empty vector, a vector targeting SRSF3 or MBNL1, or a vector encoding SRSF3, MBNL1 isoforms or Acin1$_L$ was sole- or co-transfected into HCT-116 cells, followed by incubation in growth medium supplemented with sodium arsenite (25 μM) for 24 h. Parallel TUNEL analysis were conducted as previously described.

Acknowledgments

We appreciate Dr. Christian Schwerk (University of Mahhheim) for kindly providing the expression plasmid encoding the FLAG-tagged Acin1-L isoform (pCAGGS-Acin1-L). This work was supported by a grant (MOST108–2320-B-038–034) from the Ministry of Science and Technology, Taiwan.

Supplementary materials

Supplementary material associated with this article can be found, in the online version, at doi:10.1016/j.neo.2020.10.002.

References

[1] Nilsen TW, Graveley BR. Expansion of the eukaryotic proteome by alternative splicing. *Nature* 2010;**463**:457–63.

[2] Wamsley B, Jaglin XH, Favuzzi E, Quattrocolo G, Nigro MJ, Yusuf N, et al. Rbfox1 Mediates Cell-type-Specific Splicing in Cortical Interneurons. *Neuron* 2018;**100**:846–59.

[3] Hu J, Qian H, Xue Y, Fu XD. PTB/nPTB: master regulators of neuronal fate in mammals. *Biophys Rep* 2018;**4**:204–14.

[4] Climente-Gonzalez H, Porta-Pardo E, Godzik A, Eyras E. The functional impact of alternative splicing in cancer. *Cell Rep* 2017;**20**:2215–26.

[5] Oltean S, Bates DO. Hallmarks of alternative splicing in cancer. *Oncogene* 2014;**33**:5311–18.

[6] Dvinge H, Kim E, Abdel-Wahab O, Bradley RK. RNA splicing factors as oncoproteins and tumour suppressors. *Nat Rev Cancer* 2016;**16**:413–30.

[7] Schreuders EH, Ruco A, Rabeneck L, Schoen RE, Sung JJ, Young GP, Kuipers EJ. Colorectal cancer screening: a global overview of existing programmes. *Gut* 2015;**64**:1637–49.

[8] Carethers JM, Jung BH. Genetics and genetic biomarkers in sporadic colorectal cancer. *Gastroenterology* 2015;**149**:1177–90.

[9] Eilertsen IA, Sveen A, Strømme JM, Skotheim RI, Nesbakken A, Lothe RA. Alternative splicing expands the prognostic impact of KRAS in microsatellite stable primary colorectal cancer. *Int J Cancer* 2019;**144**:841–7.

[10] Zong Z, Li H, Yi C, Ying H, Zhu Z, Wang H. Genome-wide profiling of prognostic alternative splicing signature in colorectal cancer. *Front Oncol* 2018;**8**:537.

[11] Xiong Y, Deng Y, Wang K, Zhou H, Zheng X, Si L, et al. Profiles of alternative splicing in colorectal cancer and their clinical significance: a study based on large-scale sequencing data. *EBioMedicine* 2018;**36**:183–95.

[12] Kurokawa K, Akaike Y, Masuda K, Kuwano Y, Nishida K, Yamagishi N, et al. Downregulation of serine/arginine-rich splicing factor 3 induces G1 cell cycle arrest and apoptosis in colon cancer cells. *Oncogene* 2014;**33**:1407–17.

[13] Wang JL, Guo CR, Sun TT, Su WY, Hu Q, Guo FF, et al. SRSF3 functions as an oncogene in colorectal cancer by regulating the expression of ArhGAP30. *Cancer Cell Int* 2020;**20**:120.

[14] Cheng AW, Shi J, Wong P, Luo KL, Trepman P, Wang ET, et al. Muscleblind-like 1 (Mbnl1) regulates pre-mRNA alternative splicing during terminal erythropoiesis. *Blood* 2014;**124**:598–610.

[15] Artero R, Prokop A, Paricio N, Begemann G, Pueyo I, Mlodzik M, et al. The muscleblind gene participates in the organization of Z-bands and epidermal attachments of Drosophila muscles and is regulated by DMEF2. *Dev Biol* 1998;**195**:131–43.

[16] Begemann G, Paricio N, Artero R, Kiss I, Pérez-Alonso M, Mlodzik M. Muscleblind, a gene required for photoreceptor differentiation in Drosophila, encodes novel nuclear Cys3His-type zinc-finger-containing proteins. *Development* 1997;**124**:4321–31.

[17] Goers ES, Purcell J, Voelker RB, Gates DP, Berglund JA. MBNL1 binds GC motifs embedded in pyrimidines to regulate alternative splicing. *Nucleic Acids Res* 2010;**38**:2467–84.

[18] Masuda A, Andersen HS, Doktor TK, Okamoto T, Ito M, Andresen BS, et al. CUGBP1 and MBNL1 preferentially bind to 3′ UTRs and facilitate mRNA decay. *Sci Rep* 2012;**2**:209.

[19] Tran H, Gourrier N, Lemercier-Neuillet C, Dhaenens CM, Vautrin A, Fernandez-Gomez FJ, et al. Analysis of exonic regions involved in nuclear localization, splicing activity, and dimerization of muscleblind-like-1 isoforms. *J Biol Chem* 2011;**286**:16435–46.

[20] Konieczny P, Stepniak-Konieczna E, Taylor K, Sznajder LJ, Sobczak K. Autoregulation of MBNL1 function by exon 1 exclusion from MBNL1 transcript. *Nucleic Acids Res* 2017;**45**:1760–75.

[21] Kino Y, Washizu C, Kurosawa M, Oma Y, Hattori N, Ishiura S, et al. Nuclear localization of MBNL1: splicing-mediated autoregulation and repression of repeat-derived aberrant proteins. *Hum Mol Genet* 2015;**24**:740–56.

[22] Fish L, Pencheva N, Goodarzi H, Tran H, Yoshida M, Tavazoie SF. Muscleblind-like 1 suppresses breast cancer metastatic colonization and stabilizes metastasis suppressor transcripts. *Genes Dev* 2016;**30**:386–98.

[23] Tang L, Zhao P, Kong D. Muscleblind-like 1 destabilizes Snail mRNA and suppresses the metastasis of colorectal cancer cells via the Snail/E-cadherin axis. *Int J Oncol* 2019;**54**:955–65.

[24] Tabaglio T, Low DH, Teo WKL, Goy PA, Cywoniuk P, Wollmann H, et al. MBNL1 alternative splicing isoforms play opposing roles in cancer. *Life Sci Alliance* 2018;**1**:e201800157.

[25] Lin JC, Lee YC, Liang YC, Fann YC, Kory RJ, Lin YJ. The impact of the RBM4-initiated splicing cascade on modulating the carcinogenic signature of colorectal cancer cells. *Sci Rep* 2017;**7**:44204.

[26] Nowak-Sliwinska P, van Beijnum JR, Huijbers EJM, Gasull PC, Mans L, Bex A, et al. Oncofoetal insulin receptor isoform A marks the tumour endothelium; an underestimated pathway during tumour angiogenesis and angiostatic treatment. *Br J Cancer* 2019;**120**:218–28.

[27] Matsuda Y, Hagio M, Seya T, Ishiwata T. Fibroblast growth factor receptor 2 IIIc as a therapeutic target for colorectal cancer cells. *Mol Cancer Ther* 2012;**11**:2010–20.

[28] Konieczny P, Stepniak-Konieczna E, Sobczak K. MBNL expression in autoregulatory feedback loops. *RNA Biol* 2018;**15**:1–8.

[29] Ajiro M, Jia R, Yang Y, Zhu J, Zheng ZM. A genome landscape of SRSF3-regulated splicing events and gene expression in human osteosarcoma U2OS cells. *Nucleic Acids Res* 2016;**44**:1854–70.

[30] Kino Y, Mori D, Oma Y, Takeshita Y, Sasagawa N, Ishiura S. Muscleblind protein, MBNL1/EXP, binds specifically to CHHG repeats. *Hum Mol Genet* 2004;**13**:495–507.

[31] Konieczny P, Stepniak-Konieczna E, Sobczak K. MBNL proteins and their target RNAs, interaction and splicing regulation. *Nucleic Acids Res* 2014;**42**:10873–87.

[32] Mykowska A, Sobczak K, Wojciechowska M, Kozlowski P, Krzyzosiak WJ. CAG repeats mimic CUG repeats in the misregulation of alternative splicing. *Nucleic Acids Res* 2011;**39**:8938–51.

[33] Sobczak K, Michlewski G, de Mezer M, Kierzek E, Krol J, Olejniczak M, et al. Structural diversity of triplet repeat RNAs. *J Biol Chem* 2010;**285**:12755–64.

[34] Sahara S, Aoto M, Eguchi Y, Imamoto N, Yoneda Y, Tsujimoto Y. Acinus is a caspase-3-activated protein required for apoptotic chromatin condensation. *Nature* 1999;**401**:168–73.

[35] Murachelli AG, Ebert J, Basquin C, Le Hir H, Conti E. The structure of the ASAP core complex reveals the existence of a Pinin-containing PSAP complex. *Nat Struct Mol Biol* 2012;**19**:378–86.

[36] Liu Z, Yuan G, Liu S, Jia J, Cheng L, Qi D, et al. Identified of a novel cis-element regulating the alternative splicing of LcDREB2. *Sci Rep* 2017;**7**:46106.

[37] Liu F, Dai M, Xu Q, Zhu X, Zhou Y, Jiang S, et al. SRSF10-mediated IL1RAP alternative splicing regulates cervical cancer oncogenesis via mIL1RAP-NF-κB-CD47 axis. *Oncogene* 2018;**37**:2394–409.

[38] Mai S, Qu X, Li P, Ma Q, Cao C, Liu X. Global regulation of alternative RNA splicing by the SR-rich protein RBM39. *Biochim Biophys Acta* 2016;**1859**:1014–24.

[39] Ke H, Zhao L, Zhang H, Feng X, Xu H, Hao J, et al. Loss of TDP43 inhibits progression of triple-negative breast cancer in coordination with SRSF3. *Proc Natl Acad Sci U S A* 2018;**115**:E3426–35.

[40] Kim J, Park RY, Chen JK, Kim J, Jeong S, Ohn T. Splicing factor SRSF3 represses the translation of programmed cell death 4 mRNA by associating with the 5′-UTR region. *Cell Death Differ* 2014;**21**:481–90.

[41] Lin JC, Lee YC, Tan TH, Liang YC, Chuang HC, Fann YC. RBM4-SRSF3-MAP4K4 splicing cascade modulates the metastatic signature of colorectal cancer cell. *Biochim Biophys Acta Mol Cell Res* 2018;**1865**:259–72.

[42] Liu H, Lorenzini PA, Zhang F, Xu S, Wong MSM, Zheng J, et al. Alternative splicing analysis in human monocytes and macrophages reveals MBNL1 as major regulator. *Nucleic Acids Res* 2018;**46**:6069–86.

[43] Cerro-Herreros E, Sabater-Arcis M, Fernandez-Costa JM, Moreno N, Perez-Alonso M, Llamusi B, et al. miR-23b and miR-218 silencing increase Muscleblind-like expression and alleviate myotonic dystrophy phenotypes in mammalian models. *Nat Commun* 2018;**9**:2482.

[44] Gates DP, Coonrod LA, Berglund JA. Autoregulated splicing of muscleblind-like 1 (MBNL1) Pre-mRNA. *J Biol Chem* 2011;**286**:34224–33.

[45] Hung CS, Lin JC. Alternatively spliced MBNL1 isoforms exhibit differential influence on enhancing brown adipogenesis. *Biochim Biophys Acta Gene Regul Mech* 2020;**1863**:194437.

[46] Dreumont N, Bourgeois CF, Lejeune F, Liu Y, Ehrmann IE, Elliott DJ, et al. Human RBMY regulates germline-specific splicing events by modulating the function of the serine/arginine-rich proteins 9G8 and Tra2-β. *J Cell Sci* 2010;**123**:40–50.

[47] Wang F, Wendling KS, Soprano KJ, Soprano DR. The SAP motif and C-terminal RS- and RD/E-rich region influences the sub-nuclear localization of Acinus isoforms. *J Cell Biochem* 2014;**115**:2165–74.

[48] Deka B, Singh KK. Multifaceted regulation of gene expression by the apoptosis- and splicing-associated protein complex and its components. *Int J Biol Sci* 2017;**13**:545–60.

[49] Hu Y, Yao J, Liu Z, Liu X, Fu H, Ye K. Akt phosphorylates acinus and inhibits its proteolytic cleavage, preventing chromatin condensation. *EMBO J* 2005;**24**:3543–54.